IEEE Photonics Journal
An IEEE Photonics Society Publication

Open Access

Few-Mode SDM Receivers Exploiting Parallelism of Free Space

Volume 11, Number 1, February 2019

Yongben Wang
Ningbo Zhao
Zhiqun Yang
Zhenzhen Zhang
Bin Huang
Guifang Li, *Fellow, IEEE*

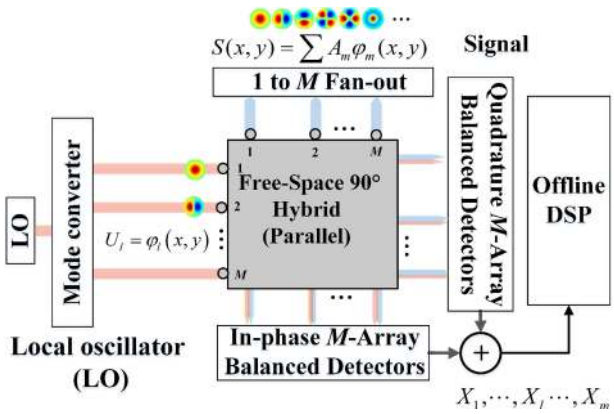

DOI: 10.1109/JPHOT.2019.2896645

Few-Mode SDM Receivers Exploiting Parallelism of Free Space

Yongben Wang [1], Ningbo Zhao,[1] Zhiqun Yang [1], Zhenzhen Zhang [1], Bin Huang [2] and Guifang Li,[1,2] *Fellow, IEEE*

[1]Key Laboratory of Opto-Electronic Information Technology of Ministry of Education, School of Precision Instrument and Opto-Electronics Engineering, Tianjin University, Tianjin 300072, China
[2]CREOL, The College of Optics and Photonics, University of Central Florida, Orlando, FL 32816 USA

DOI:10.1109/JPHOT.2019.2896645

Manuscript received November 26, 2018; revised January 17, 2019; accepted January 27, 2019. Date of publication January 31, 2019; date of current version February 14, 2019. This work was supported in part by the National Natural Science Foundation of China under Grants 61335005 and 61775165.
Corresponding authors: Ningbo Zhao and Guifang Li (e-mail: nbzhao@tju.edu.cn; li@creol.ucf.edu).

Abstract: Few-mode receivers exploiting parallelism of free space for space-division multiplexed (SDM) transmission, in which one free-space 90° optical hybrid can be shared among multiple SDM channels, are proposed and experimentally demonstrated. A 2×20 Gb/s quadrature phase-shift keying two-mode mode-division multiplexed receiver has been demonstrated experimentally.

Index Terms: Optical fiber communication, coherent receiver, mode-division multiplexed.

1. Introduction

The capacity of single-mode fibers (SMFs) is rapidly approaching the limit imposed by the combination of Shannon's information theory and nonlinear effects in optical fibers [1]. Space-division multiplexing (SDM) is a promising technology to overcome the capacity limit of conventional SMF. Mode-division multiplexed (MDM) transmission in few-mode fibers (FMFs), which utilizes the multiplicity of modes to increase the data-carrying capacity, is one of promising approaches to overcome this limitation [2]–[3]. So far, MDM transmission experiments up to 15 modes in FMFs have been demonstrated [4]–[7]. Alternatively, multi-core fibers (MCF) and few-mode MCFs can also be used for SDM. 6-mode MCFs with more than one hundred total spatial channels have been reported [8].

For all the MDM transmission experiments reported so far, mode multiplexers and demultiplexers using phase plates [9], photonic lanterns [10] and multi-plane light converters [11] are indispensable at the receiver. In such a receiver, the required number of single-mode 90° hybrids equals to the number of spatial channels. As the spatial degree of freedom M increases, the circuit size for these single-mode 90° hybrids increases linearly, which could place a heavy burn on integrated SDM/MDM receivers as each individual 90° hybrid occupies a significant area. For instance, in [12], the size of photonic integrated circuit (PIC) composed of a 90° hybrid and four photodiodes is 1.6×4.1 mm, most of which was occupied by the 90° hybrid. Even with recent advances in silicon-based PIC technology [13]–[15], the accumulation of these hybrids in SDM/MDM receivers will become a challenge as the number of spatial modes scales up.

The insertion loss (IL) of (de)multiplexers increases as the number of spatial modes scales up. Mode conversion in combination with passive combing using phase plates or spatial light modulators was used in early-stage MDM experiments. However, these devices suffer from large IL from passive beam combining. The photonic lanterns have much lower IL [16], which increases as the number of spatial modes scales up. In addition, as the adiabatic requirement for smooth transition of high-order modes is more difficult to achieve, the mode-dependent loss (MDL) increases as the number of mode scales [17]. The IL and MDL for mode (de)multiplexers based on multi-plane light conversion (MPLC) also scale with the number of modes [18], [19]. In this paper, we propose and demonstrate a few-mode coherent receiver that requires only one free-space 90° optical hybrid, taking advantage of the parallelism of free space and potentially the recently demonstrated high-speed two-dimensional detector arrays [20]. We present two approaches to compensate the fundamental splitting loss (SL) and compared the performances of these approaches using the Gaussian-noise (GN) model. We prove the feasibility of our proposal by demonstrating a two-spatial-mode few-mode receiver.

This paper is organized as follows. Section 2 summarizes the theory of the proposed few-mode SDM receivers. Section 3 presents the approaches to compensate the IL and splitting loss. Sections 4 and 5 provide experimental setup and results, respectively, of the proposed receiver. Section 5 concludes the paper.

2. Theory

For a classical MDM transmission system, the MDM signals containing M modes need to be demultiplexed using mode demultiplexers. After the mode demultiplexer, possibly followed by pre-amplification and filtering, M separated signals are injected into M single-mode receivers, respectively. Obviously, the number of single-mode 90° hybrids required equals to the number of spatial modes. The proposed MDM receiver uses only one free-space 90° hybrid, exploiting parallelism of free-space.

The schematics of the proposed MDM receivers are shown in Fig. 1 for one polarization. Scheme A is shown in Fig. 1(a) in which the MDM signals are separated into fundamental modes by using a mode demultiplexer. A local oscillator (LO) in the fundamental mode is fanned out into copies by using a passive beam splitter (BS). To measure the complex field of light, a free-space optical hybrid is used to combine each of the signal branches and LO branches.

Because its aperture can be made almost arbitrarily larger, one free-space 90° hybrid can accommodate many single-mode inputs. Therefore, it is possible to use only one free-space 90° hybrid for receiving MDM signals from multiple FMFs and/or few-mode MCFs. For the case of N FMFs, the number of mode demultiplexers is N. For the case of MCF having N few-mode cores, $N \times M$ core-mode demultiplexing is necessary, which not only introduces insertion loss but also can be expensive.

In view of this, we propose an alternative scheme B shown in Fig. 1(b). The main differences are that 1) a BS is used instead of the mode demultiplexer to split the MDM signal into M identical copies, and 2) each branch of LOs contained one of the modes used for MDM transmission and is derived from a fundamental-mode source through mode conversion. In this approach, the transmitted MDM signals can be expressed as:

$$S(x, y) = \sum A_m \varphi_m (x, y) \tag{1}$$

where the subscript m is the spatial mode index; A_m and $\varphi_m(x, y)$ are the amplitude and the normalized mode profile of the m-th mode, respectively. Thus, the optical field of the l-th branch after splitting can be expressed as:

$$S_l(x, y) = \frac{1}{\sqrt{M}} \sum A_m \varphi_m(x, y) \tag{2}$$

The optical field of the l-th branch of the LOs is given:

$$U_l(x, y) = \varphi_l(x, y) \tag{3}$$

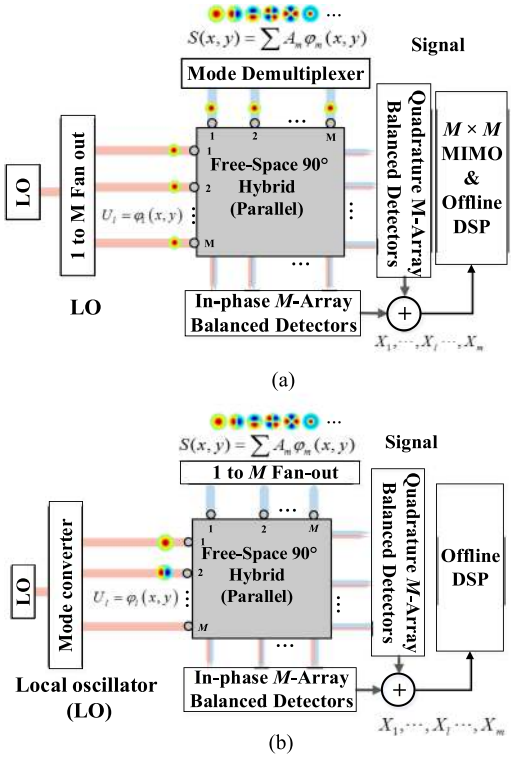

Fig. 1. Schematics of two few-mode coherent receivers. (a) With a mode demultiplexer (Scheme A). (b) Without the mode demultiplexer and with a power splitter (Scheme B).

It should be pointed out that the IL associated with this mode transformation on the LOs is not as critical as that of the demultiplexers in standard MDM receivers because the local oscillator laser power is usually not a limiting factor. In view of this, the $1/\sqrt{M}$ splitting loss was ignored in Eq. (3), in addition to the fact that the standard MDM receivers would need either M independent LO lasers or one LO laser split into M paths. To measure the complex field of optical field, a free-space 90° hybrid was used in this receiver. The interference between the MDM signal and the LOs are converted into photocurrents at the free-space photodetectors (PDs) with areas designed to be larger the spot sizes of the MDM signals and the LOs. In so doing, the orthogonality of spatial modes is maintained when integrated over the surface of the PDs,

$$\delta_{mn} = \iint \varphi_m(x,y)\varphi_n^*(x,y)dxdy \tag{4}$$

Finally, the in-phase and quadrature component of the photocurrents resulting from the l-th branch can be derived as:

$$\begin{aligned} i_{l,I} &\propto \iint (S_l U_l^* + S_l^* U_l)dxdy \\ i_{l,Q} &\propto \iint j(-S_l U_l^* + S_l^* U_l)dxdy \end{aligned} \tag{5}$$

Using the orthogonality condition in Eq. (4) and combining photocurrents in all the PDs, the received complex amplitudes resulting from the l-th branch including in-phase and quadrature can be derived as:

$$X_l = i_{l,I} + j i_{l,Q} = \frac{1}{\sqrt{M}} A_l \tag{6}$$

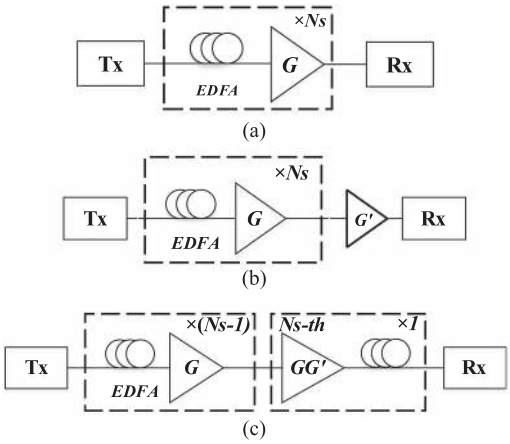

Fig. 2. Schematic of three long-haul optically amplified transmission systems. (a) A typical long-haul optically amplified system, (b) a long-haul optically amplified system with a pre-amplifier, and (c) a long-haul optically amplified system with an increased gain of last EDFA. N_s is the number of spans.

The photocurrents are first digitized and then the signal streams A_m are extracted by the following digital signal processing, as will be shown below.

Since the only signal that is detected on the photodetector is what overlaps with the LO mode, the $1 \times M$ beam splitter introduces a fundamental splitting loss (SL), of $1/M$ compared to using a mode demultiplexer. As the spatial degree of freedom M increases, the SL can make this approach impractical. In the next section, we evaluate whether it is possible to effectively compensate the $1/M$ fundamental SL as well as the IL of mode demultiplexers.

3. Compensation for the IL of Mode Demultiplexers and Fundamental SL of Splitters

The proposed receiver (scheme B) is specially designed for multiple FMFs/few-mode MCFs optically-amplified long-haul systems. The receivers of schemes A and B suffer from unavoidable IL of mode demultiplexers and fundamental SL, respectively. In order to maintain the minimum OSNR and input power into the receiver, the IL of mode demultiplexers and the fundamental SL must be compensated.

We start from a baseline single-carrier long-haul optically transmission system without any excess loss as shown in Fig. 2(a) and consider approaches for compensating the IL of mode demultiplexers in Fig. 1(a) and/or the fundamental SL in Fig. 1(b). One approach is to add a pre-amplifier to provide a gain (equals to the IL or SL) at the receiving end of this long-haul optically amplified systems, as is shown in Fig. 2(b). Alternatively, increase the gain of the last Erbium-doped fiber amplifier (EDFA) from G to GG', in Fig. 2(c). In both cases, $G' = IL$ or $G' = SL$. Obviously, the approach in Fig. 2(b) will introduce additional amplified spontaneous emission (ASE) noise while the second approach in Fig. 2(b), although will not increase the number of EDFAs, will introduce both ASE and the nonlinear noise originating from nonlinear interference (NLI) in the last span, and all of them can contribute to OSNR degradation.

Therefore, the Gaussian noise (GN) model is utilized to analyze the system performance differences between Fig. 2(a) and 2(b) or Fig. 2(a) and 2(c), respectively [21]. The linear noise comes from the ASE of EDFAs. The ASE power spectral density (PSD) for each amplifier in two polarizations is given by:

$$N_{ASE} \approx 2n_{sp}h\nu_0 G = NFh\nu_0 G \tag{7}$$

where NF is the noise figure of each EDFA, h and ν_0 are the Plank's constant and frequency, respectively. According to the theory of EDFA, the noise figure of each EDFA can be expressed as:

$$NF = \frac{2n_{sp}\,(G\ -\ 1)}{G} \tag{8}$$

where n_{sp} is the population inversion factor of EDFA. According to the GN model, the nonlinear noise originating from NLI can be well approximated as additive white Gaussian noise (AWGN). The NLI scales linearly with the number of spans and $P_{ch,tx}$ is the launched power per channel. The NLI power introduced in each fiber span can be expressed as [22]:

$$N_{NLI} \cong \eta P_{ch,tx}^3 \tag{9}$$

Where η is the normalized NLI efficiency which depends on the parameters of the link and signal, and independent of the modulation format, according to [22]:

$$\eta \approx \frac{8}{27}\gamma^2 L_{eff}^{\ 2}\,\frac{a\,\sinh\left(\frac{\pi^2}{2}\,|\beta_2|\,L_{eff,a}N_{ch}^2R_s^2\right)}{\pi\,|\beta_2|\,L_{eff,a}R_s^2} \tag{10}$$

where γ is the fiber nonlinear coefficient, β_2 is the dispersion parameter, L_{eff} is effective length defined as $L_{eff} = \frac{1-\exp(-\alpha L)}{\alpha}$, $L_{eff,a} = 1/\alpha$ is the asymptotic effective length, N_{ch} is the number of channels and R_s is effective bandwidth. And then the total noise for all N_s fiber spans at the receiver can be expressed as:

$$N_{total} = N_s\,(N_{ASE} + N_{NLI}) \tag{11}$$

For the ideal system in Fig. 2(a), the system performance is governed by the OSNR which includes both ASE and nonlinear noise contributions as follows:

$$OSNR_a = \frac{P_{ch,tx}}{N_s(N_{ASE} + \eta P_{ch,tx}^3)} \tag{12}$$

Moreover, minimizing the bit error ratio (BER) at a fixed distance is accomplished by maximizing the OSNR. According to the [21], the launch power per channel which maximizes OSNR is readily found as:

$$P_{ch,opt,a} = \sqrt[3]{\frac{N_{ASE}}{2\eta}} \tag{13}$$

If $P_{ch,opt,a}$ is inserted back into Eq. (12), it is immediately seen that the overall ASE noise term at the denominator is always twice the overall NLI noise term. In other words, the maximum OSNR is always obtained when $N_{ASE} = 2P_{NLI}$. The result, was first pointed out in [23] and then experimentally confirmed in [24].

Similarly, when adding a pre-amplifier with a gain G' to compensate the IL or SL in Fig. 2(b), the modified OSNR in this transmission system can be expressed as:

$$OSNR_b = \frac{P_{ch,tx}}{N_s\left(N_{ASE} + \eta P_{ch,tx}^3\right) + N'_{ASE}} \tag{14}$$

where N'_{ASE} is the ASE noise introduced by the pre-amplifier. According to Eq. (7), the ASE resulting from the pre-amplifier is given by:

$$N'_{ASE} = \left(G'/G\right) N_{ASE} \tag{15}$$

For simplicity, assuming $G'/G = K$. For this system in Fig. 2(b), we also can obtain the optimal launch power per channel which can maximize OSNR:

$$P_{ch,opt,b} = \sqrt[3]{\frac{N_s + K}{N_s}\cdot\frac{N_{ASE}}{2\eta}} \approx P_{ch,opt,a} \tag{16}$$

Therefore, we can obtain the OSNR penalty resulting from adding the pre-amplifier at the receiving end as:

$$OSNR\_Penalty_b = \frac{OSNR_a}{OSNR_b} = \frac{P_{ch,tx}}{N_s\left(N_{ASE} + \eta P_{ch,tx}^3\right)} \cdot \frac{N_s\left(N_{ASE} + \eta P_{ch,tx}^3\right) + N'_{ASE}}{P_{ch,tx}}$$

$$= 1 + \frac{1}{N_s}\left(\frac{K}{1 + \frac{\eta P_{ch,tx}^3}{N_{ASE}}}\right) \tag{17}$$

With reference to the Eq. (16), the penalty of OSNR in Fig. 2(b) can be re-written as:

$$OSNR\_Penalty_b = 1 + \frac{2K}{3N_s} \tag{18}$$

Similarly, for the second approach, when the gain of the last EDFA is changed to GG', as shown in Fig. 2(c), the modified OSNR of the link can be expressed as:

$$OSNR_c = \frac{P_{ch,tx}}{(N_s - 1)\left(N_{ASE} + \eta P_{ch,tx}^3\right) + \left(N'_{ASE} + \eta P'^3_{ch,tx}\right)} \tag{19}$$

where $P'^3_{ch,tx}$ is the input power into the $N_s th$ fiber span is given by:

$$P'_{ch,tx} = G' P_{ch,tx} = K G P_{ch,tx} \tag{20}$$

For this system in Fig. 2(c), we also can obtain the optimal launch power per channel which can maximize OSNR as:

$$P_{ch,opt,c} = \sqrt[3]{\frac{(N_s - 1 + G')}{(N_s - 1 + G'^3)} \cdot \frac{N_{ASE}}{2\eta}} = \sqrt[3]{\frac{N_s - 1 + G'}{N_s - 1 + G'^3}} \cdot P_{ch,opt,a} \tag{21}$$

Similarly, we also can obtain the OSNR penalty resulting from the change in the gain of the $N_s th$ EDFA as,

$$OSNR\_Penalty_c = \frac{OSNR_a}{OSNR_c} = \frac{P_{ch,opt,a}}{N_s\left(N_{ASE} + \eta P_{ch,opt,a}^3\right)} \cdot \frac{(N_s - 1)\left(N_{ASE} + \eta P_{ch,opt,c}^3\right) + \left(N'_{ASE} + \eta P'^3_{ch,opt,c}\right)}{P_{ch,opt,c}}$$

$$= \frac{P_{ch,opt,a}}{P_{ch,opt,c}} \frac{2(N_s - 1 + G') + (N_s - 1 + G'^3)\left(\frac{P_{ch,opt,a}}{P_{ch,opt,c}}\right)^3}{3N_s} \tag{22}$$

According to the optimum input power mentioned above, the OSNR penalty for Fig. 2(c) can be re-written as:

$$OSNR\_Penalty_c = \sqrt{\frac{N_s - 1 + G'^3}{N_s - 1 + G'}} \frac{N_s - 1 + G'}{N_s} = \sqrt[3]{\frac{29 + (KG)^3}{29 + KG}} \frac{29 + (KG)}{30} \tag{23}$$

Equations (18) and (23) represent the OSNR penalties of the first approach in Fig. 2(b) and the second approach in Fig. 2(c), respectively. For each compensation approach above, the difference in OSNR penalty between compensating the IL of mode demultiplexers (scheme A) and the fundamental SL (scheme B) is an important reference, and is shown in Fig. 3(a) and (3b) for 3 modes ($SL = 1/3$ *or* 4.77 dB) and 6 modes ($SL = 1/6$ *or* 7.78 dB), respectively., and is shown in Fig. 3(a) and (3b) for 3 modes ($SL = 1/3$ *or* 4.77 dB) and 6 modes ($SL = 1/6$ *or* 7.78 dB), respectively. These optically-amplified long-haul transmission systems have the following parameters: the total length is 3000 km, the length of each span is 100 km, and the fiber loss coefficient is $\alpha_{dB} = 0.2$ dB/km. So, the number of spans is $N_s = 30$, the gain of each EDFA is $G = 100$ *or* 20 dB.

It can be seen from Fig. 3(a) and (3b) that, as the IL of mode demultiplexers increases, the difference in OSNR penalty for 3 and 6 modes decreases slowly. Furthermore, the results of the

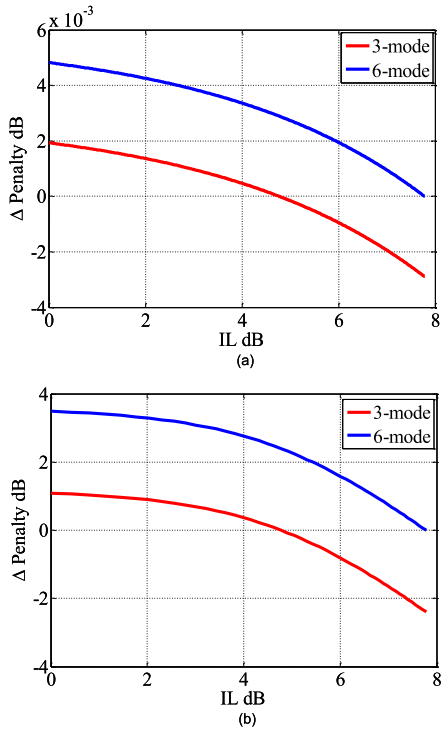

Fig. 3. The relation of IL of mode demultiplexers and the difference of OSNR penalty. (a) The first compensation approach in Fig. 2(b). (b) The second compensation approach in Fig. 2(c).

first approach in Fig. 3(a) indicate that the difference in OSNR penalty is negligibly small regardless of the IL of mode demultiplexers. Also, in the limit of $K \ll 1$, which is the case for the range of the plots, the penalty in Eq. (18) can be approximated as a linear correlation while it does not exist in Eq. (23).

Although it seems that the first approach by adding a pre-amplifier in scheme B increases the complexity of the receiver, we save the number of mode demultiplexers at the receiving end for MDM transmission systems using multiple FMFs or MCFs. Assuming there are N FMFs or the MCF has N few-mode cores, the complexity of scheme B is equivalent to one power splitter and N EDFAs. In contrast, scheme A would require N mode demultiplexers or $N \times M$ core-mode demultiplexers. This is because that one free-space splitter in scheme B can be used for many FMFs or MCFs with many few-mode cores each carrying MDM signals. Therefore, scheme B is especially advantageous for SDM systems using multiple FMFs or MCFs.

4. Experimental Setup

The schematic of the experimental setup for scheme B is shown in Fig. 4. At the transmitter, an external cavity laser (ECL) with a linewidth of 100 kHz operating at 1550 nm was modulated by a 10 Gbaud pseudorandom binary sequence (PRBS) (of length $2^{15} - 1$) using a quadrature phase-shift keying (QPSK) modulator. The signal is then selectively launched into an FMF by a mode multiplexer after appropriate decorrelation using an optical delay line. The mode multiplexer is a free-space multiplexer using phase plates, as shown in Fig. 4. It consists of two fiber collimators (FCs), a passive BS and a phase plate for mode conversion. And then an EDFA followed by a variable optical attenuator (VOA) in each tributary was used to equalize the launch power before the FMF. For this proof-of-concept experiment, it is sufficient to demonstrate demultiplexing of two modes: the fundamental mode LP_{01} and the second-order mode LP_{11a}. Some mode coupling of

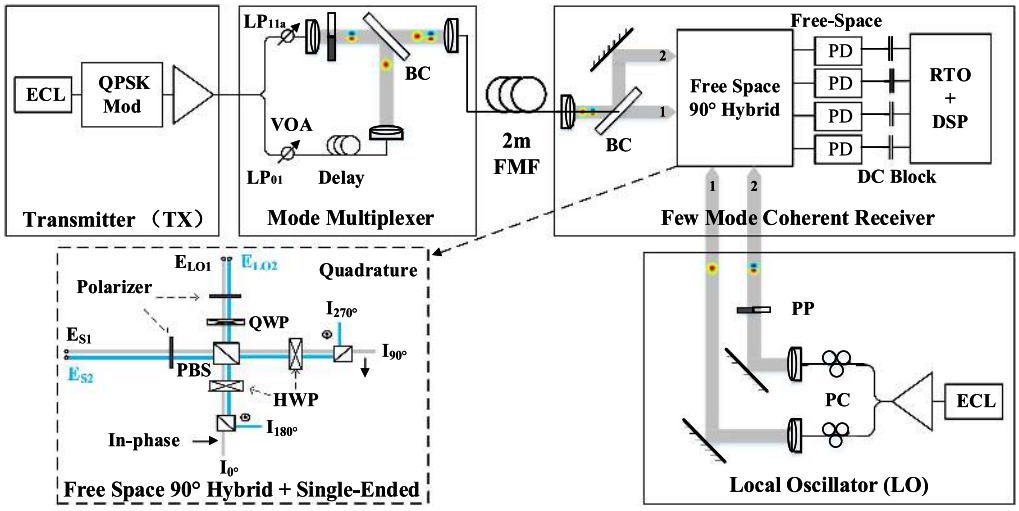

Fig. 4. Schematic of experimental setups of a 2 × 20 Gb/s mode-division multiplexed BTB transmission system for scheme B. ECL: external cavity laser; VOA: variable Optical Attenuator; BC: beam combiner, PBS: polarization beam splitter, PD: photodetector; PC: polarization controller; PP: phase plate; HWP: half wave plate; QWP: quarter wave plate; RTO: real time oscilloscope.

the multiplexer and the 2-m FMF is unavoidable but can be neglected because it is not a dominant problem.

At the local oscillator side, the same type ECL is used. A phase plate is placed into one of the two light paths to generate the LP_{11a} mode. As is shown in Fig. 4, we designed the special coherent detection experiment setup. Here we demonstrate single-polarization receiving, where the LO laser was aligned in the polarization of the transmitted signal. The current scheme can be easily extended for polarization multiplexing using a polarization-diversity approach. We construct a free-space 90° optical hybrid capable of supporting multiple beams synchronously. We rotate the polarization controllers (PCs) to align with the orthogonal polarization state in accordance with the signal before being combined by the free-space 90°optical hybrid.

The free-space 90° optical hybrid is constructed, as shown in Fig. 4, containing one quarter wave plate (QWP), two half wave plates (HWP), and three polarization beam splitters (PBS). The 90° phase shift, between the signal and LOs, is introduced by the QWP. The number of spatial degrees of freedom (# of fibers/cores × # modes per fiber/core) that can be accommodated by a single free-space hybrid is equal to the aperture area of the hybrid divided by the area of a single MDM beam in free space. Due to the limited number of high-speed free-space photodetectors, we used single-ended detection, instead of balanced detection presented in Section 3. For this system, we will need to measure 2 complex quantities that are linearly independent. And these two measurements were accomplished using 4 single-ended detectors: one complex quantity used the 0° & 90° outputs of the hybrid and the other used the 180° & 270° outputs of the hybrid.

The first approach (scheme A) demultiplex the MDM signal first by a mode demultiplexer, and then beat the resulting single-mode outputs with single-mode local oscillators in one free-space 90° optical hybrid. A simple single-mode back-to-back (BTB) transmission experiment was performed to verify the feasibility of this hybrid. To some degree, the single-mode experiment can be used to verify the feasibility of scheme A in Fig. 1(a), also regarded as a comparative reference.

5. Experimental Results

In our experiment, the received signal power of each beam before arriving at the surface of each PD is set to 0 dBm by using VOAs. The mixed optical signal was detected by four single-ended

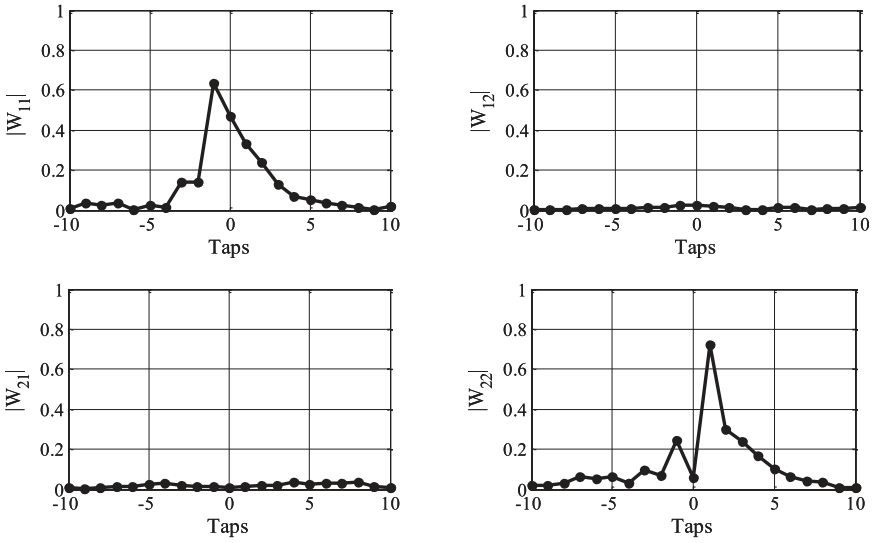

Fig. 5. The sub-filter coefficients in the time-domain for the 2×20 Gb/s MDM-QPSK transmission system ($LP_{01} + LP_{11a}$).

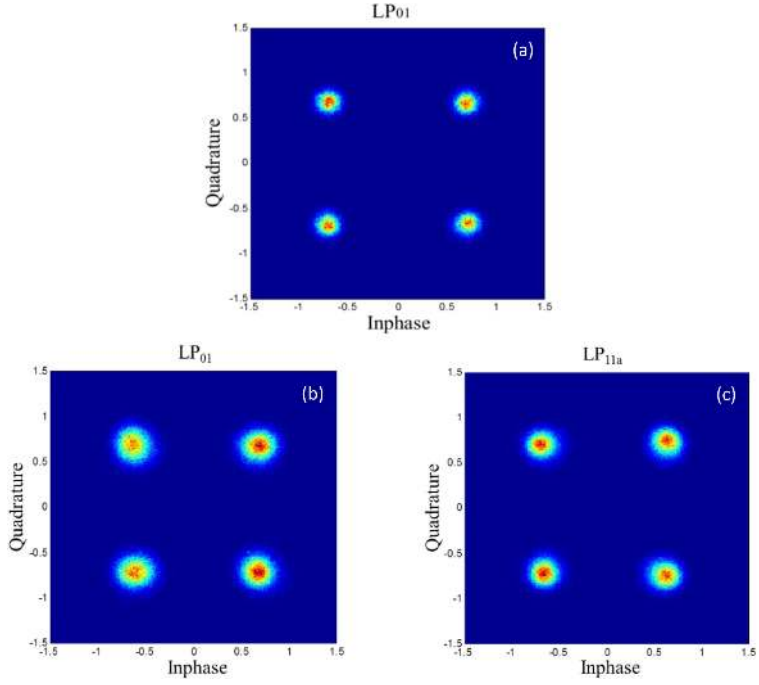

Fig. 6. Constellations of BTB transmission system. (a) LP_{01} channel for the single-mode transmission. (b) LP_{01} and (c) LP_{11a} for the 2×20 Gb/s MDM-QPSK transmission.

free-space PDs, the bandwidth and responsibility of which is 12.5 GHz and 0.88 A/W, respectively. The four DC blocks are applied to filter out the DC components of the detected signals.

After detection, the four signals from the free-space PDs are digitized by analog-to-digital converters (ADC) [25] at 80 Gsamples/s with a 36 GHz electrical bandwidth. The sampled waveforms are processed off-line. The digital signal processing steps include: (i) down-sampling to 20 Gsamples/s (ii) adaptive butterfly structure with filter coefficients determined using the constant modulus

algorithm (CMA) in the electronic domain, (iii) frequency offset estimation, (iv) phase recovery, and (v) bit-error decisions.

The magnitude of the sub-filter coefficients in the time domain for the 2×20 Gb/s MDM-QPSK transmission system ($LP_{01} + LP_{11a}$) after CMA convergence is plotted in Fig. 5. Fig 6(b) and (6c) show constellation diagrams of two channels for LP_{01} and LP_{11a} of BTB transmission system for after total signal processing. By the digital signal process above, the Q^2-factor of channel LP_{01} and LP_{11a} are 14.9 dB and 14.3 dB, respectively. The bit errors of the LP_{01} channel and the LP_{11a} channel are counted and the two channels are both error free.

As a reference, Fig. 6(a) shows the constellation of single-mode BTB transmission using the same free-space optical hybrid, under the same experimental conditions. After digital signal processing, the Q^2-factor of the LP_{01} channel is 16.5 dB, about 1.6 dB higher than the above. This is probably because that the offset between the centers of the signal and LO beams, the imperfect orthogonality between LP_{01} and LP_{11a} modes in practical experiment is negligible.

Also, the losses of phase plates for mode conversion and unavoidable mode coupling could contribute to the Q^2-factor degradation. Nevertheless, experimental results verify the validity of the proposed method.

6. Conclusions and Discussions

In conclusion, we propose and experimentally demonstrate few-mode SDM receivers using only one free-space 90° optical hybrid. We demonstrated the feasibility of the proposed method by receiving a 2×20 Gb/s MDM signal using the proposed receiver, yielding results consistent with theory. The first approach (scheme A) demultiplex the MDM signal first, and then beat the resulting single-mode outputs with single-mode local oscillators in one free-space 90° optical hybrid. This approach has the advantages of 1) each path involves only single-mode Gaussian beams having small spot size, 2) large-bandwidth single-mode balanced detectors can be used. In contrast, the second approach (scheme B) split the MDM signal first and then beat each copy of the MDM signal with one of the modes. This approach has the advantages of 1) free-space splitters in general will have lower insertion losses than that of mode demultiplexers, and 2) one free-space splitter can be used for multiple FMFs or MCFs with many few-mode cores each carrying MDM signals. In essence, scheme B allows space parallelism across multiple FMFs/MCF cores while the scheme A allows for higher speed detection and more modes.

The advantage of the proposed few-mode SDM receivers is their scalability not only in terms of the number of modes multiplexed on each wavelength as demonstrated here, but also in terms of the number of wavelength channels for wavelength-division multiplexed (WDM) MDM transmission. This is because the 90° optical hybrid is mode- and wavelength-independent. As long as they have large enough aperture sizes, they can accommodate all wavelength-mode channels. When the number of wavelength-mode channels becomes large, exploiting the parallelism of the three-dimensional free space may offer advantages over two-dimensional integration using planar photonic integrated circuits. This is especially advantageous for SDM systems when the number of FMFs or MCF cores becomes large.

References

[1] R. J. Essiambre, G. Kramer, P. J. Winzer, G. J. Foschini, and B. Goebel, "Capacity limits of optical fiber networks," *J. Lightw. Technol*, vol. 28, no. 4, pp. 662–701, Feb. 2010.
[2] D. J. Richardson, J. M. Fini, and L. E. Nelson, "Space-division multiplexing in optical fibres," *Nat. Photon.*, vol. 7, no. 5, pp. 354–362, 2013.
[3] G. Li, N. Bai, N. Zhao, and C. Xia, "Space-division multiplexing: The next frontier in optical communication," *Adv. Opt. Photon.*, vol. 6, no. 4, pp. 413–487, 2014.
[4] N. Bai and G. Li, "Adaptive frequency-domain equalization for mode-division multiplexed transmission," *IEEE Photon. Technol. Lett.*, vol. 24, no. 21, pp. 1918–1921, Nov. 2012.
[5] X. Chen, A. Li, J. Ye, A. Al Amin, and W. Shieh, "Reception of mode-division multiplexed superchannel via few-mode compatible optical add/drop multiplexer," *Opt. Exp.*, vol. 20, no. 13, pp. 14302–14307, 2012.

[6] R. Ryf *et al.*, "Mode-division multiplexing over 96 km of few-mode fiber using coherent 6 × 6 MIMO processing," *J. Lightw. Technol.*, vol. 30, no. 4, pp. 521–531, Feb. 2012.
[7] N. K. Fontaine *et al.*, "30 × 30 MIMO transmission over 15 spatial modes," in *Proc. Opt. Fiber Commun. Conf. Exhib.*, 2015, Paper Th5C.1.
[8] K. Igarashi *et al.*, "Ultra-dense spatial-division-multiplexed optical fiber transmission over 6-mode 19-core fibers," *Opt. Exp.*, vol. 24, no. 10, pp. 10213–10231, 2016.
[9] C. Montero-Orille *et al.*, "Ion-exchanged glass binary phase plates for mode-division multiplexing," *Appl. Opt.*, vol. 52, pp. 2332–2339, 2013.
[10] N. K. Fontaine, R. Ryf, J. Bland-Hawthorn, and S. G. Leon-Saval, "Geometric requirements for photonic lanterns in space division multiplexing," *Opt. Exp.*, vol. 20, no. 24, pp. 27123–27132, 2012.
[11] G. Labroille, J. Pu, N. Barré, B. Denolle, and J. F. Morizur, "Recent progress in mode multiplexing devices using multi-plane light conversion," in *Proc. 21st Opto Electron. Commun. Conf., 2016 Int. Conf. Photon. Switch.*, 2016, Paper S2–2.
[12] H. Yagi, M. Takechi, M. Kurokawa, Y. Fujimura, Y. Tateiwa, and Y. Yoneda, "64 Gbaud high-bandwidth micro intradyne coherent receiver using high-efficiency and high-speed InP-based photodetector integrated with 90° hybrid," in *Proc. Opt. Fiber Commun. Conf. Exhib.*, 2017, Paper Th1A.2.
[13] K. Xu *et al.*, "Light emission from a poly-silicon device with carrier injection engineering," *Mater. Sci. Eng., B*, vol. 231, pp. 28–31, 2018.
[14] M. Morschbach, M. Oehme, and E. Kasper, "Visible light emission by a reverse-biased integrated silicon diode," *IEEE Trans. Electron Dev.*, vol. 54, no. 5, pp. 1091–1094, May 2007.
[15] K. Xu, "Monolithically integrated Si gate-controlled light-emitting device: Science and properties," *J. Opt.*, vol. 20, no. 2, 024014: 1-8, 2018.
[16] S. G. Leon-Saval, N. K. Fontaine, J. R. Salazar-Gil, B. Ercan, R. Ryf, and J. Bland-Hawthorn, "Mode-selective photonic lanterns for space-division multiplexing," *Opt. Exp.*, vol. 22, no. 1, pp. 1036–1044, 2014.
[17] B. Huang *et al.*, "10-Mode photonic lanterns using low-index micro-structured drilling preforms," in *Opt. Fiber Commun. Conf. Exhib.*, 2017, Paper Tu3J.5.
[18] G. Labroille *et al.*, "Characterization and applications of spatial mode multiplexers based on multi-plane light conversion," *Opt. Fiber Technol.*, vol. 35, pp. 93–99, 2017.
[19] N. Barré, B. Denolle, P. Jian, J. F. Morizur, and G. Labroille, "Broadband, mode-selective 15-mode multiplexer based on multi-plane light conversion," in *Proc. Opt. Fiber Commun. Conf. Exhib.*, 2017, Paper Th3E.5.
[20] T. Umezawa *et al.*, "10-GHz 32-pixel 2-D photodetector array for advanced optical fiber communications," in *Proc. Conf. Lasers Electro-Opt.*, 2017, Paper SF2I.1.
[21] P. Poggiolini, "The GN model of non-linear propagation in uncompensated coherent optical systems," *J. Lightw. Technol.*, vol. 30, no. 24, pp. 3857–3879, Dec. 2012.
[22] M. Nazarathy *et al.*, "Phased-array cancellation of nonlinear FWM in coherent OFDM dispersive multi-span links," *Opt. Exp.*, vol. 16, pp. 15778–15810, 2008.
[23] G. Bosco, A. Carena, R. Cigliutti, V. Curri, P. Poggiolini, and F. Forghieri, "Performance prediction for WDM PM-QPSK transmission over uncompensated links," in *Proc. Opt. Fiber Commun. Expo., Nat. Fiber Opt. Eng. Conf.*, Mar. 2011, Paper OThO7.
[24] F. Vacondio *et al.*, "On nonlinear distortions of highly dispersive optical coherent systems," *Opt. Exp.*, vol. 20, no. 2, pp. 1022–1032, Jan. 2012.
[25] R. H. Walden, "Analog-to-digital converter survey and analysis," *IEEE J. Sel. Area. Commun.*, vol. 17, no. 4, pp. 539–550, Apr. 1999.